Electronic Supplementary Material (ESI) for Nanoscale.

Correlation between Hysteresis Dynamics and Inductance in Hybrid Perovskite Solar Cells: Studying the Dependency on ETL/Perovskite Interface

Rana Yekani,* Hsien-chieh Chiu, Dallas Strandell, Zhuoran Wang, Stéphanie Bessette,[a] Raynald Gauvin,[a] Patanjali Kambhampati, [b] George P. Demopoulos *[a]

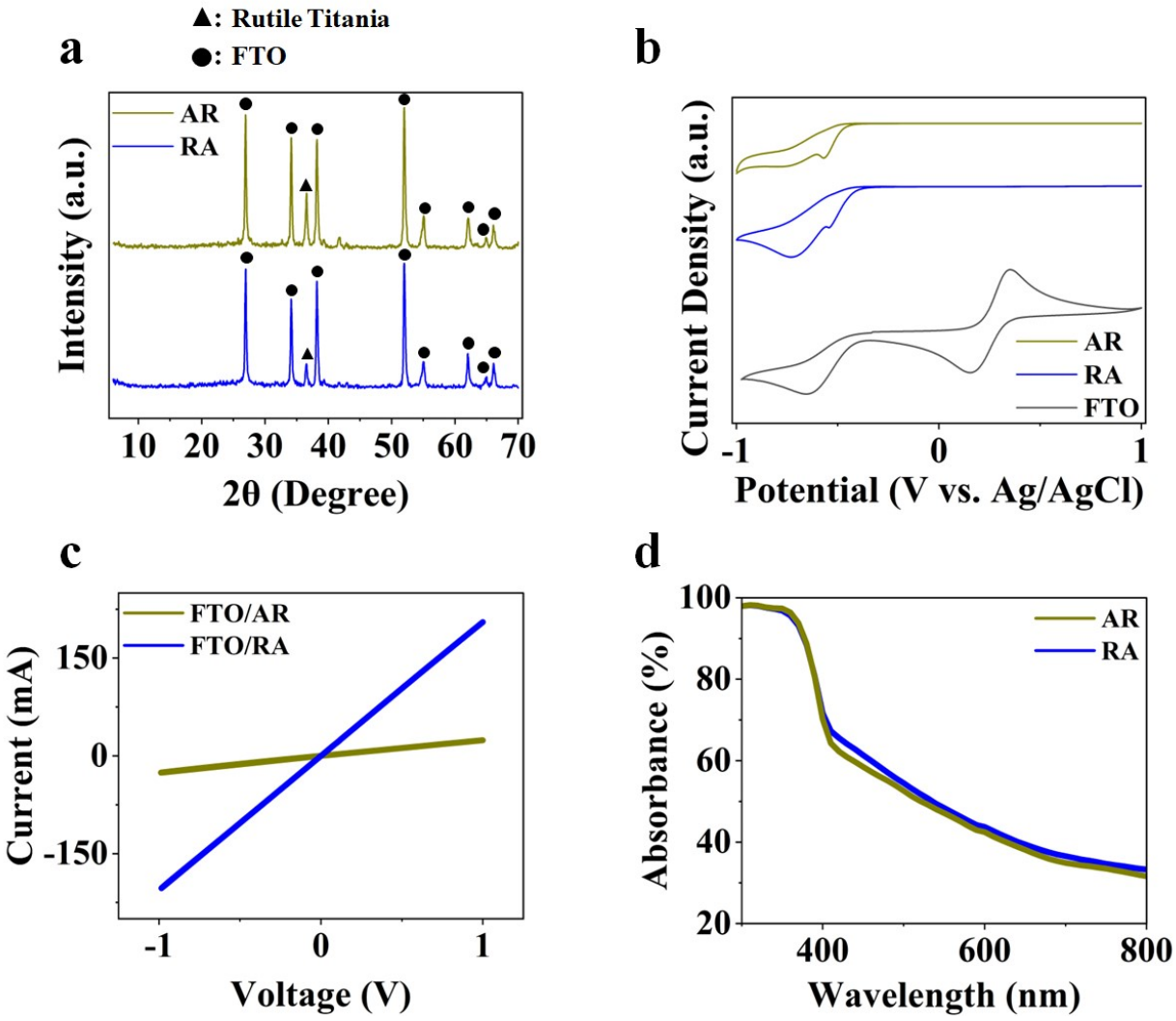

Figure S1- a) XRD patterns (peaks marked by filled triangle and circle denote diffraction from rutile titania and FTO, respectively), b) cyclic voltammetry scans, (c) effective conductivity of the ETL structures, (d) the UV-Vis absorbance spectra. All the presented results are obtained over FTO/ETL stacks.

Supplementary Note 1:

The single diffraction peak corresponding to titania, conform with the tetragonal rutile phase of P42/mnm space group (JCPDS No. 88-1175, a=b=0.4517 nm and c=0.2940 nm). This peak corresponds to the [001] direction, which is the theoretically preferential growth direction for rutile titania nanorods[1, 2]. Since spray pyrolysis typically results in very thin layers[3], the corresponding peaks could not be detected in our XRD patterns. However, deposition of titania through spray pyrolysis is known to produce anatase phase[4, 5].

Supplementary Note 2:

The effective conductivity of FTO/ETL stacks is obtained from the slope associated with each trend line according to: $\sigma = \frac{I}{V} = \frac{I}{R}$. σ is calculated to be 206.05 S for FTO/RA and 24.63 S for FTO/AR.

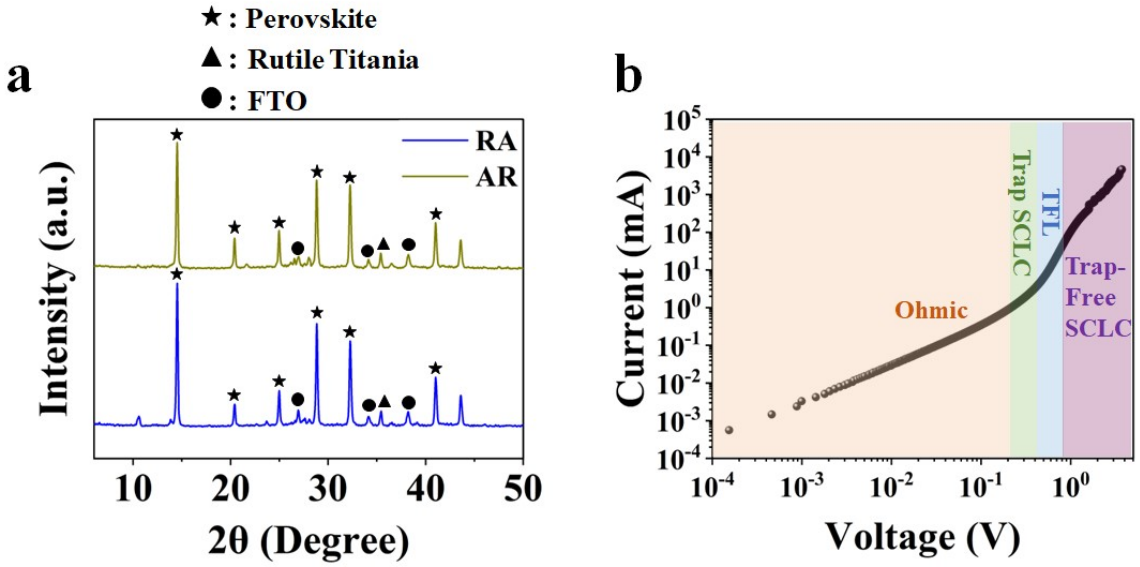

Figure S2- (a) XRD pattern of the perovskite layer infiltrating AR and RA ETL structures. (b) dark current- voltage curve for FTO/spiro-OMeTAD/Au architecture.

Table S1- PV metrics variation of PSCs based on AR and RA ETL structure for forward scan (FS) and reverse scan (RS), under 100 and 10 mV/s scan rates. The champion device in each case is highlighted in the row underneath.

	J_{SC} (RS)	V_{OC} (RS)	FF (RS)	PCE(RS)	J_{SC} (FS)	V_{OC} (FS)	FF (FS)	PCE (FS)
100 mV/s AR	21.16 ± 0.56	1.017 ± 0.01	73.36 ± 2.48	15.81 ± 1.02	21.16 ± 0.52	0.97 ± 0.01	71.39 ± 3.25	14.67 ± 0.94
Champion Device	21.88	1.041	75.01	17.09	21.77	0.985	72.51	15.55
10 mV/s AR	20.98 ± 0.55	1.035 ± 0.014	72.44 ± 2.24	15.75 ± 0.95	21.01 ± 0.51	0.999 ± 0.01	68.97 ± 2.04	14.49 ± 0.76
Champion Device	21.88	1.058	73.88	17.10	21	1.019	73.21	15.66
100 mV/s RA	21.91 ± 0.89	1.06 ± 0.02	72.5 ± 2.88	16.90 ± 1.43	21.80 ± 0.75	1.036 ± 0.01	69.67 ± 4.71	15.75 ± 1.40
Champion Device	22.88	1.10	77.61	19.66	22.22	1.073	75.95	18.10
10 mV/s RA	21.03 ± 0.81	1.06 ± 0.02	72.34 ± 2.70	16.27 ± 1.21	21.01 ± 0.82	1.05 ± 0.02	65.57 ± 4.32	14.51 ± 1.46
Champion Device	22.11	1.10	78.46	19.22	22.11	1.08	72.51	17.44

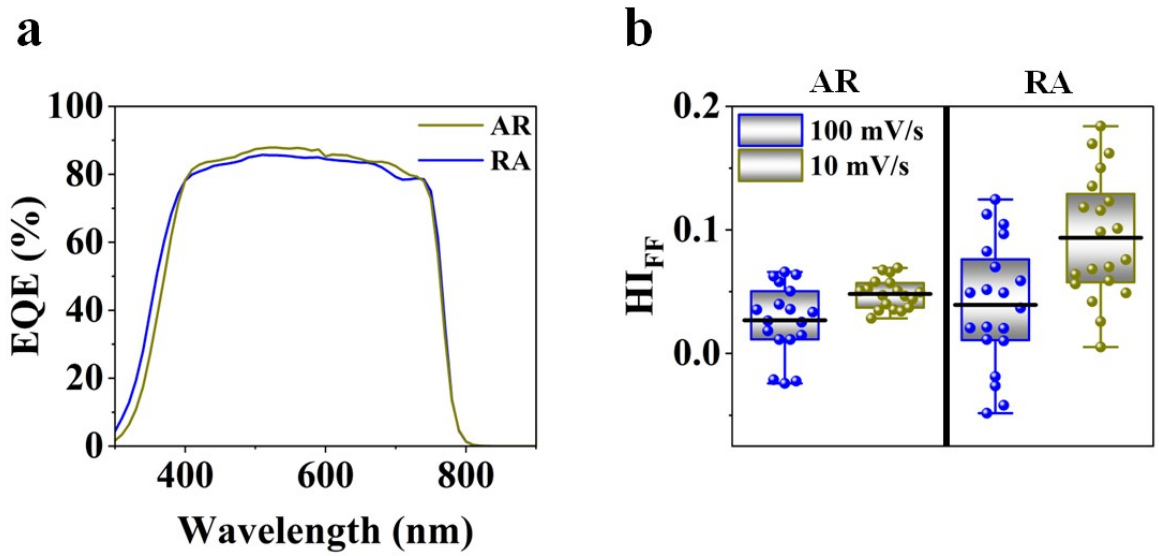

Figure S3- (a) EQE spectra obtained for PSCs based on AR and RA ETL structures (b) Distribution of HI_{FF} for PSCs based on AR and RA ETL structures.

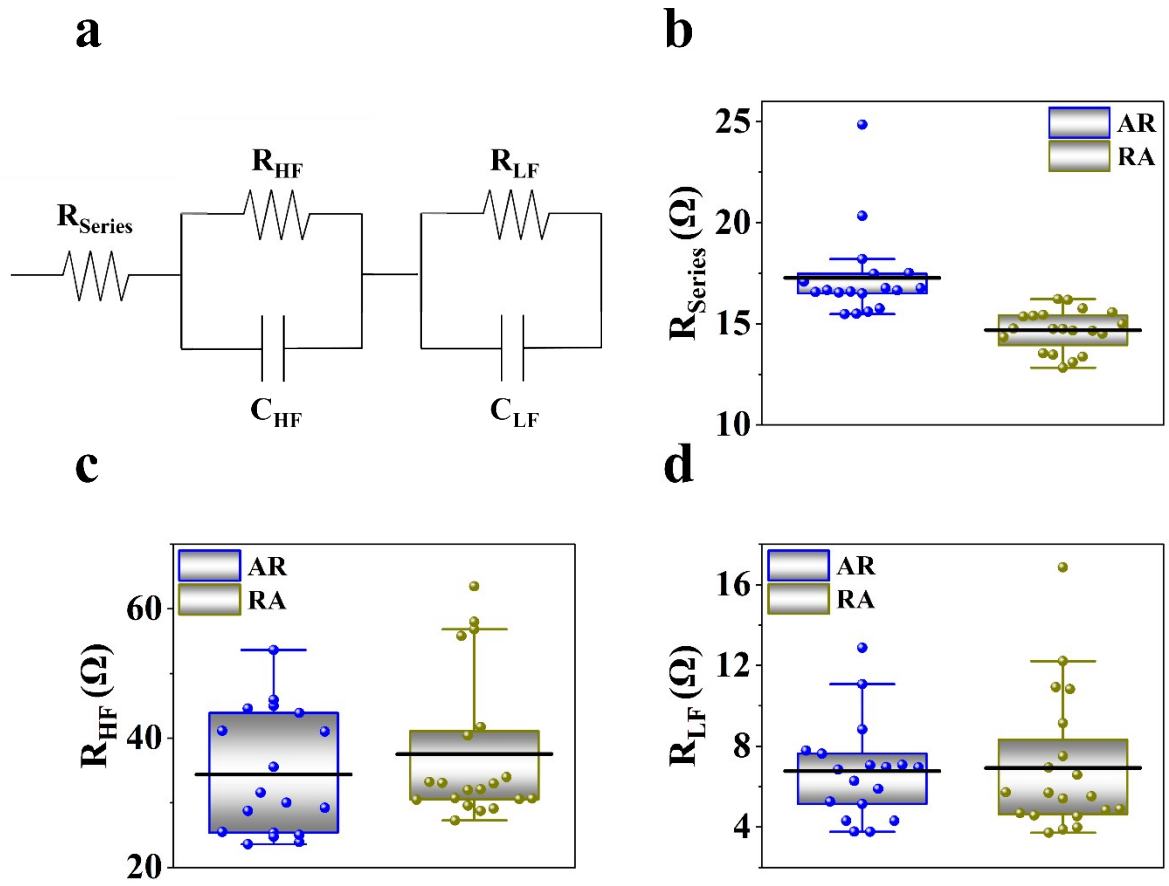

Figure S4- (a) Equivalent circuit used for fitting the EIS spectra recorded under open-circuit condition, comparison of (b) $R_{Series,}$ (c) R_{HF}, and (d) R_{LF} for PSCs based on AR and RA.

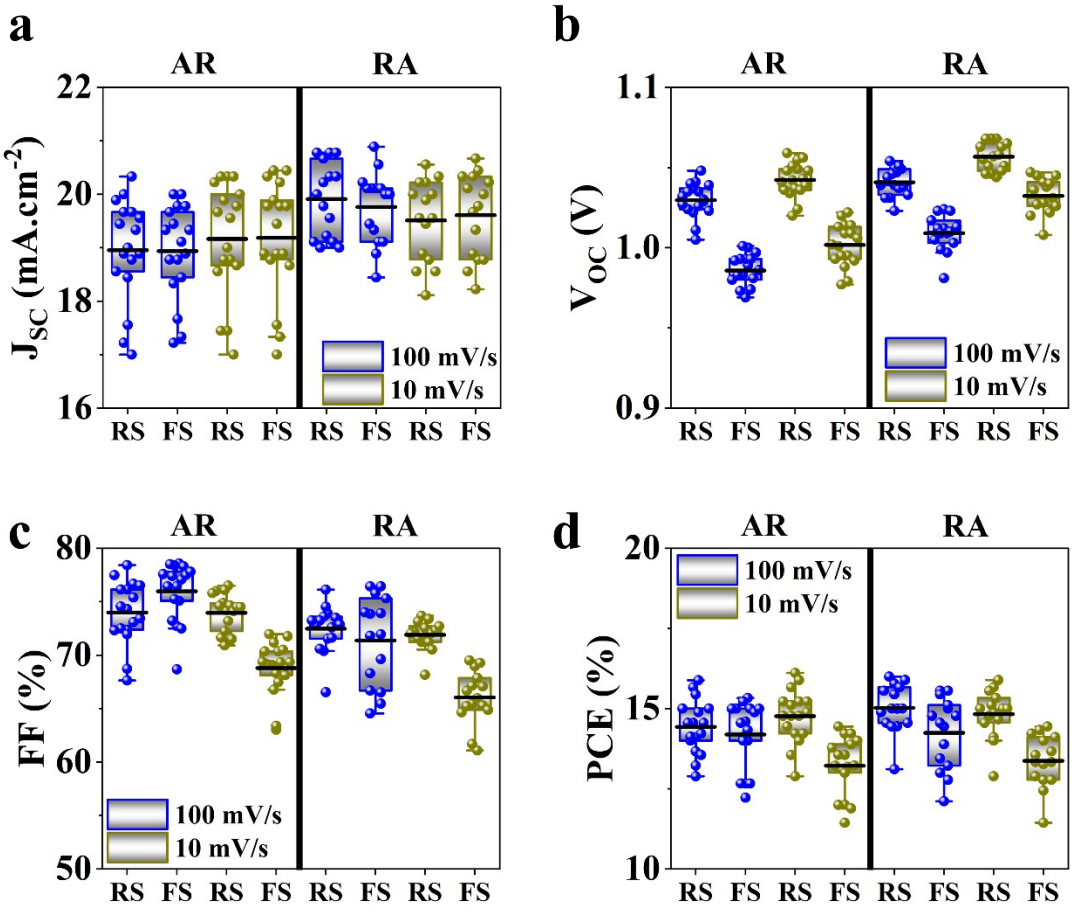

Figure S5- The distribution of PV metrics after storing the devices for 200 hours under dark and 25% relative humidity: (a) J_{SC}, (b) V_{OC}, (c) FF, (d) PCE

Table S2- PV metrics variation of PSCs based on AR and RA ETL structure for forward scan (FS) and reverse scan (RS), under 100 and 10 mV/s scan rates, corresponding to storing the devices for 200 hours under dark and 25% relative humidity. The champion device in each case is highlighted in the row underneath.

	J_{SC} (RS)	V_{OC} (RS)	FF (RS)	PCE(RS)	J_{SC} (FS)	V_{OC} (FS)	FF (FS)	PCE (FS)
100 mV/s AR	18.95 ± 0.93	1.029 ± 0.01	73.97 ± 2.84	14.43 ± 0.81	18.93 ± 0.86	0.985 ± 0.009	75.96 ± 2.67	14.19 ± 0.991
Champion Device	19.33	1.048	78.41	15.88	19.66	0.992	77.58	15.22
10 mV/s AR	19.16 ± 1.05	1.042 ± 0.01	73.94 ± 1.71	14.76 ± 0.8	19.18 ± 1.04	1.001 ± 0.01	68.95 ± 2.45	13.21 ± 0.87
Champion Device	19.88	1.059	76.49	16.11	19.88	1.009	71.97	14.44
100 mV/s RA	19.91 ± 0.67	1.04 ± 0.008	72.43 ± 2.13	15.02 ± 0.72	19.76 ± 0.65	1.009 ± 0.01	71.37 ± 4.04	14.24 ± 1.06
Champion Device	20.77	1.046	73.61	15.99	20.11	1.012	76.43	15.55
10 mV/s RA	19.51 ± 0.73	1.056 ± 0.008	71.89 ± 1.298	14.82 ± 0.723	19.60 ± 0.76	1.032 ± 0.01	66.04 ± 2.38	13.37 ± 0.79
Champion Device	20.55	1.063	72.71	15.88	20.33	1.03	68.96	14.44

References

1. J. Kalb, J. A. Dorman, S. Siroky and L. J. C. Schmidt-Mende, *Crystals* 2019, **9**, 64.
2. A. Wisnet, S. B. Betzler, R. V. Zucker, J. A. Dorman, P. Wagatha, S. Matich, E. Okunishi, L. Schmidt-Mende, C. J. C. G. Scheu and Design, *Crystal Growth & Design*, 2014, **14**, 4658-4663.
3. M. Saliba, T. Matsui, J. Y. Seo, K. Domanski, J. P. Correa-Baena, M. K. Nazeeruddin, S. M. Zakeeruddin, W. Tress, A. Abate, A. Hagfeldt and M. Gratzel, *Energy Environ Sci*, 2016, **9**, 1989-1997.
4. A. Conde, M. Guerrero, N. Castillo, A. B. Soto, R. Fragoso and J. Cabanas-Moreno, *Thin Solid Films*, 2005, **473**, 68-73.
5. A. M. E. Raj, V. Agnes, V. Bena Jothy, C. Ravidhas, J. Wollschläger, M. Suendorf, M. Neumann, M. Jayachandran and C. Sanjeeviraja, *Thin Solid Films*, 2010, **519**, 129-135.